Ferroelectrics

ISSN: 0015-0193 (Print) 1563-5112 (Online) Journal homepage: https://www.tandfonline.com/loi/gfer20

Pressure-Induced Phase Transitions in ScF 3 Crystal--Raman Spectra and Lattice Dynamics

K. S. Aleksandrov , V. N. Voronov , A. N. Vtyurin , S. A. Goryainov , N. G. Zamkova , V. I. Zinenko & A. S. Krylov

To cite this article: K. S. Aleksandrov , V. N. Voronov , A. N. Vtyurin , S. A. Goryainov , N. G. Zamkova , V. I. Zinenko & A. S. Krylov (2003) Pressure-Induced Phase Transitions in ScF 3 Crystal--Raman Spectra and Lattice Dynamics, Ferroelectrics, 284:1, 31-45, DOI: 10.1080/00150190390204691

To link to this article: https://doi.org/10.1080/00150190390204691

Published online: 22 Jan 2011.

Ferroelectrics, 2003, Vol. 284, pp. 31–45
Reprints available directly from the publisher
Photocopying permitted by license only
DOI: 10.1080/00150190390204691

Pressure-Induced Phase Transitions in ScF_3 Crystal—Raman Spectra and Lattice Dynamics

K. S. ALEKSANDROV,[1] V. N. VORONOV,[1] A. N. VTYURIN,[1]
S. A. GORYAINOV,[2] N. G. ZAMKOVA,[1] V. I. ZINENKO,[1]
and A. S. KRYLOV[1]

[1]*Kirensky Institute of Physics, Krasnoyarsk, 660036 Russia*
[2]*Joint Institute for Geology, Geophysics and Mineralogy, Novosibirsk, 630090 Russia*

(Received June 25, 2002)

New pressure-induced phases are found in normally cubic ScF_3 crystal using polarizing microscopy and micro-Raman spectroscopy. Their supposed space groups are $R3c$, $Z = 2$ and $Pnma$, $Z = 4$. Using *ab initio* model cubic phase was shown to be stable at ambient pressure down to $T = 0$ K, while hydrostatic pressure brings one of the phonon branches down to negative squared frequencies. R_5 soft mode condensation results in the rhombohedric distortion of the cubic lattice with cell volume doubling. Calculated squared frequencies of the high pressure phase are positive, their number and values agree with experimental results.

Keywords: ScF_3; high pressure; phase transitions; Raman scattering; *ab initio* lattice dynamics

PACS: 61.50.Ks; 63.70.+h; 64.70 Kb; 78.30.−j

INTRODUCTION

Fluorides with ideal or distorted α-ReO_3 structure belong to the perovskite-like crystal family, where one of the cations' positions is vacant (Fig. 1). Like many other perovskites, they show a sequence of phase transitions under pressure or temperature changes (see, e.g., [1–3]). ScF_3 seems to be the least studied of them; it was not mentioned in the most complete reviews [2, 3] of perovskite system properties, while PDF database gives three different structures for it [4]: cubic, rhombohedric and orthorhombic. Special investigations of these phases' stability [5] showed, that the orthorhombic phase is metastable at ambient conditions, while the cubic phase was not found at all. In [3, 6, 7] crystals of this structure were noted as highly sensitive to structural defects, imperfections and intrinsic strains (due to high temperature

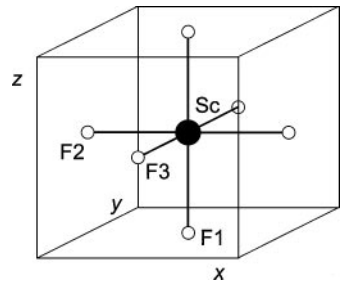

Figure 1. Structure of ScF_3 cubic phase.

melt growth), that could considerably reconstruct phase diagrams, and may explain such variegated data.

Earlier [8, 9] we've reported about successful growing of cubic ScF_3 crystal using lower temperature flux melt technique, but in contrast to its isomorphs it did not reveal any phase transitions down to 4 K. So we've performed this investigation of cubic ScF_3 under high hydrostatic pressure using micro-Raman spectroscopy. Results are interpreted in the framework of *ab initio* model of ionic crystal lattice dynamics.

SAMPLES SYNTHESIS AND STRUCTURE

Samples of ScF_3 were grown by flux-melt technique, analogous to the one for FeF_3 and AlF_3 [10–12]; its main merit is lower temperature of the melt that provides less intrinsic strains. LiF was used as a solvent; several other fluorides were tried as well, but they give too tiny crystals (less than 1 mm^3).

Flux melt containing 40% of ScF_3 was placed into platinum ampoule (with 0.2 mm walls) and sealed in nitrogen atmosphere. This ampoule was lowered down the vertical tube furnace (axial temperature gradient 1–2 K/mm) from 1400 K region at 20 mm a day speed during 14 days.

After cooling we've found there a cylindrical sample; its lower part of 10 mm diameter and 7 mm height was transparent and free of defects or inclusions visible under a microscope. X-ray scattering showed its single phase structure in good agreement with cubic structure of ScF_3 [4] with $a_0 =$ 4.01 Å unit cell parameter. Polarizing microscopy showed optical isotropy of the crystal that agrees with its cubic symmetry as well.

MICRO-RAMAN SPECTROSCOPY

Vibrational representation for the cubic phase at the center of Brillouin zone is:

$$\Gamma_0 = F_{2u} + 3F_{1u}, \tag{1}$$

and all these vibrations are Raman inactive.

Analogous representation for the rhombohedric phase:

$$\Gamma_1 = \mathbf{A_{1g}} + 2A_{2g} + \mathbf{3E_g} + 2A_{1u} + 3A_{2u} + 5E_u, \tag{2}$$

and for the orthorhombic one:

$$\Gamma_2 = \mathbf{7A_g} + \mathbf{5B_{1g}} + \mathbf{7B_{2g}} + \mathbf{5B_{3g}} + 5A_u + 7B_{1u} + 5B_{2u} + 7B_{3u}. \tag{3}$$

In (2) and (3) Raman active presentations are given in bold. As it's clearly seen from (1)–(3), Raman selection rules for these phases differ considerably, and they could be easily recognized by their Raman spectra.

Samples of ScF_3 were studied under high (up to 9 GPa) hydrostatic pressure and room temperature using diamond anvil cell [13, 14], with 0.25 mm active volume diameter and 0.1 mm height. Pressure was measured (within 0.05 GPa precision) by ruby luminescence line shift [14, 15]; ruby microcrystal was placed into the cell with the sample. Usual ethanol-methanol mixture or dehydrated glycerol were used as pressure transferring liquids. Raman spectra were exited by Ar^+ (514,5 nm, 0.5 W) laser and registered with multichannel OMARS 89 (Dilor) Raman spectrometer with nitrogen-cooled CCD detector. Due to strong diffuse background scattering only higher (150–600 cm^{-1}) part of the spectra were studied. At the same time we've observed crystal birefringence under optical polarizing microscope.

In accordance with (1) there are no Raman active lines at ambient pressure for this crystal; it is optically isotropic and could be easily darkened under microscope with crossed polarizers (at higher pressure some birefringence appears in diamond anvils due to anisotropic mechanical stress). Two Raman lines, at 260 cm^{-1} and 465 cm^{-1} (Fig. 2), appear above 0.7 GPa; at the same pressure optical anisotropy reveals under the microscope (Fig. 3). Some samples show big (0.02–0.05 mm) domains of irregular shape. At further compressing lines' intensity grows, and lower line shifts to the higher frequencies, up to 300 cm^{-1} at 3.8 GPa. One more line appears at lower part of the spectra, that moves monotonically from 180 cm^{-1} at 1.4 GPa

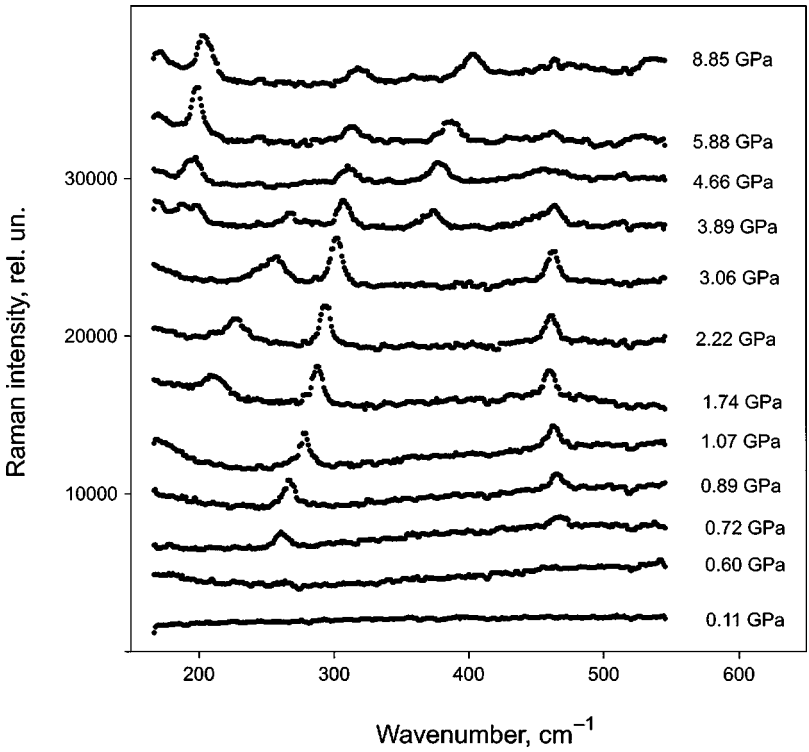

Figure 2. Transformation of ScF_3 Raman spectrum under pressure increase.

to 260 cm^{-1} at 3.8 GPa. Optical anisotropy grows as well showing bright interference colors.

All changes observed up to 3.8 GPa are reversible and can be reproduced with different samples or different pressure transferring liquids. No hysteresis effects were found within mentioned precision of pressure measurements (Fig. 4). Domain structure can differ depending on a sample quality or compressing pace. Mainly it depends on the defects at the sample boundaries; for well cut microcrystals single domain state can be easily obtained.

Under further compression one more transition has been observed at 3.8 GPa. Complicated system of smaller (less than 0.01 mm) domains appears in the crystal; it is clearly seen under the microscope and results in strong light scattering (Fig. 5). Raman spectrum changes simultaneously—several new lines and bands appear (Figs. 3 and 4). This transition point agrees well

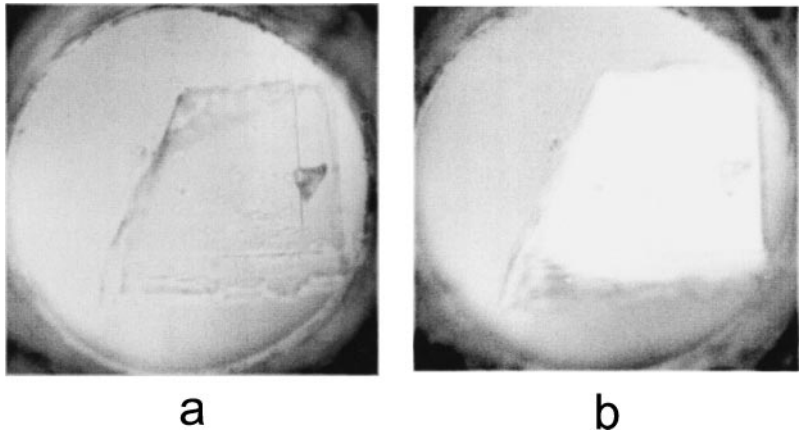

Figure 3. Sample of ScF_3 before (to the left, 0.07 GPa) and after (to the right, 0.72 GPa) the first transition point. Polarizers are crossed. High pressure cell diameter is 0.25 mm.

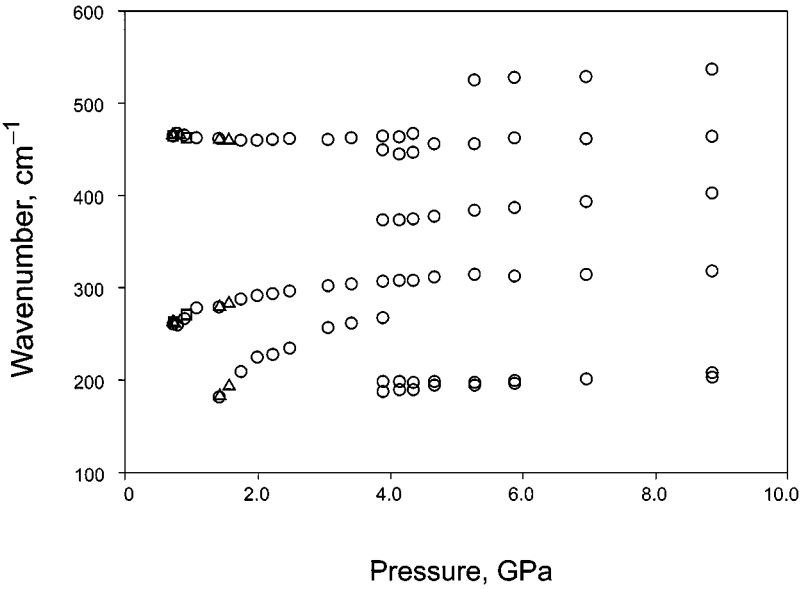

Figure 4. Pressure dependence of Raman lines' frequencies. Circles—data obtained under pressure increase, squares and triangles—pressure decrease from the second phase, with different samples.

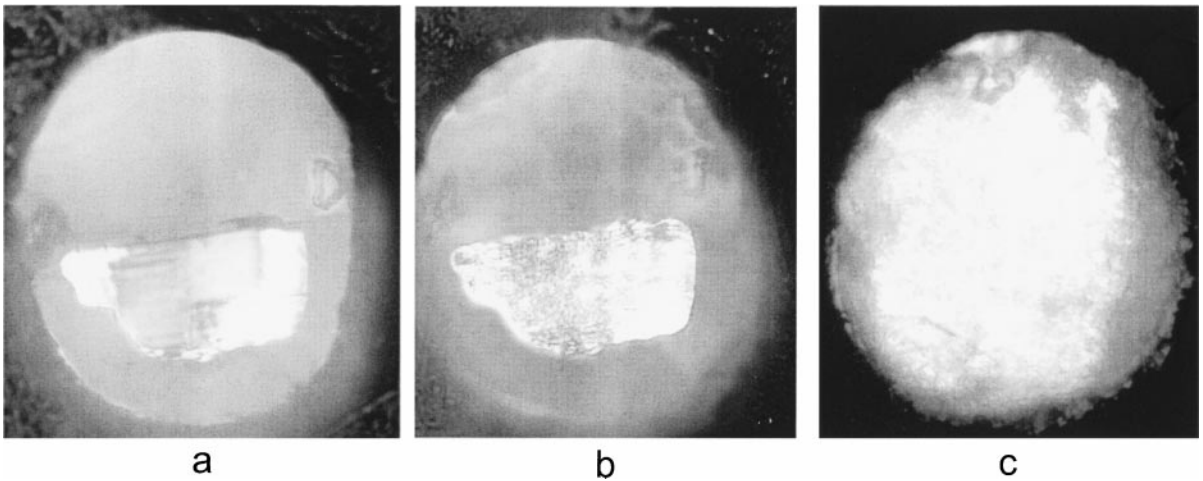

Figure 5. Sample of ScF_3 before (a, 3.06 GPa) and after (b, 3.89 GPa) the second phase transition, and after its destruction due to quick decompression (c, 0.1 GPa).

with the one, observed earlier in [7] and interpreted as the rhombohedric—orthorhombic transition.

Under further pressing higher (above 200 cm^{-1}) part of the spectrum changes not so much while at lower frequencies one of the lines shifts up crossing with another one, and probably one more line appears near 160 cm^{-1} above 7 GPa.

New domain structure modifies slightly under pressing: domains grow and their number decreases, but they never disappear. The crystal remains optically anisotropic though strong light scattering due to numerous domain walls embarrasses observations.

Decompressing of this phase does not result in the backward transition (Fig. 6). This domain walls system and general character of Raman spectra stay intact, though one lower frequency line softens slightly, that may be due

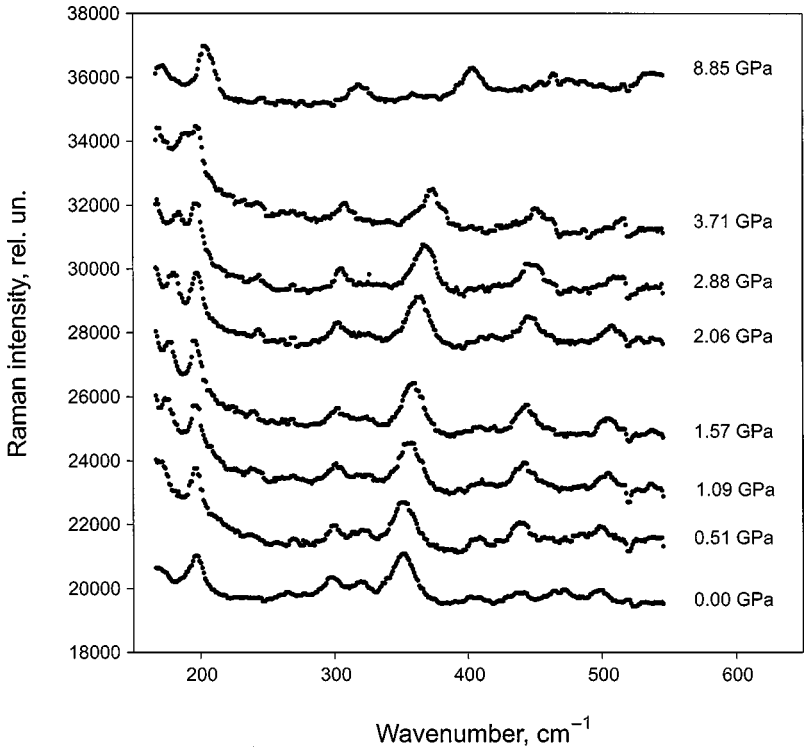

Figure 6. Transformation of ScF_3 Raman spectrum under pressure decrease from the orthorhombic high-pressure phase.

to some lattice softening. Under slow (in several hours) decompressing the sample may be kept intact down to ambient pressure—the last spectrum in Fig. 6 was obtained with the sample brought to open air. Faster decompressing below 1 GPa results in sample destruction (Fig. 5c).

LATTICE DYNAMICS SIMULATIONS

To simulate ScF_3 lattice dynamics we've build *ab initio* model, based on Gordon-Kim approximation with account for ionic deformity and polarizability [16]; details of computations are given in [17]. Earlier this approach was used to simulate lattice dynamics of several MeF_3 crystals (AlF_3, GaF_3, InF_3) and stability of their cubic phases was demonstrated.

Calculated parameters of cubic ScF_3 lattice are given in Table I; equilibrium cell parameter was determined by crystal energy minimization with respect to crystal volume, and this value was used to calculate ionic polarizabilities, dynamic charges, and dielectric permittivity ε_∞ of the crystal. Obtained cell parameter agrees well (within 5%) with the experimental value. Effective charge tensor for Sc^{3+} ion is isotropic, in accordance with its site symmetry, and its value is close to nominal ionic charge. For fluorine ions this tensor has two independent components that correspond to longitudinal ($Z^*_{\parallel,F}$) and transversal ($Z^*_{\perp,F}$) Sc–F interactions.

Calculated phonon spectrum of the cubic phase is given in Fig. 7. There are no imaginary frequencies in the spectrum (that agrees well with lattice stability down to 4 K), but one branch, from *R* to *M* point of Brillouin zone, shows extremely low frequency, with very weak dispersion along *R*–*M* line. Triply degenerated R_5 mode of this branch, as well as non-degenerated modes in *R*–*M* direction, including *M* point, corresponds to fluorine displacements [18]. Most phase transitions in perovskite-like halides, including MeF_3 crystals (*Me* = Al, Ga, In . . .), are connected with this mode condensation [1, 2].

To simulate effects of crystal compression on lattice dynamics, phonon spectrum was calculated at non-equilibrium, smaller cell parameter values. Corresponding pressure was estimated in two ways: by numerical

TABLE I Calculated parameters of ScF_3 cubic phase

a_0 (Å) exper.	a_0 (Å) calc.	Z^*_{Sc}	$Z^*_{\parallel F}$	$Z^*_{\perp F}$	α_{Sc} (Å^3)	α_F (Å^3)	ε_∞	C_{11} (GPa)	C_{12} (GPa)	C_{44} (GPa)	B (GPa)
4,01	3,82	3,36	−0,71	−1,95	0,27	0,72	1,75	172,7	18,9	18,6	70,2

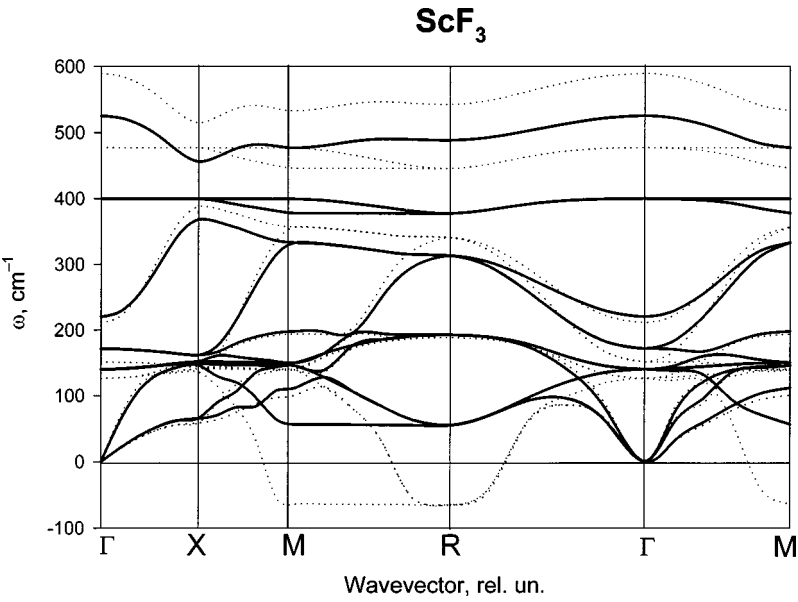

Figure 7. Calculated phonon dispersions for ScF_3 cubic phase. Full line—for cell parameter $a = 7.22$ a. u. (ambient pressure), dotted line—$a = 7.06$ a. u.

differentiation of crystal energy over its volume, and from bulk elastic modulus $B = (C_{11} + 2C_{12})/3$, where elastic constants were calculated from acoustic phonons' dispersion at $\mathbf{q} \to 0$ (given in Table I). Obtained equation of state is plotted in Fig. 8, and phonon dispersion curves calculated at cell volume 52.1 Å^3 (that corresponds to $P \approx 6$ GPa) are presented in Fig. 7. It's clearly seen from this figure that higher frequency modes harden under pressure applied, while the lowest R–M branch softens making cubic phase unstable.

DISCUSSION

In accordance with experimental results [8, 9] our simulations confirm stability of ScF_3 cubic lattice at ambient pressure down to $T = 0$ K. At the same time both experimental results obtained here and lattice dynamics calculations reveal lattice instability of this crystal under hydrostatic pressure applied. According to the model simulations, triple degenerated mode R_5 from the point $R = \frac{\pi}{a}(1, 1, 1)$ of Brillouin zone appears soft, and it seems

TABLE II Compatibility relations and calculated frequencies for cubic and rhombohedral phases of ScF_3 (Experimental frequencies are given in brackets)

Cubic phase			Rhombohedral phase	
Frequency (cm^{-1})	Irreducible representation		Irreducible representation	Frequency (cm^{-1})
590	F_{1u} – LO	$\longrightarrow$	A_{2u}	557
477	F_{1u} – TO	$\longrightarrow$	E_u	442
154	F_{1u} – LO	$\longrightarrow$	A_{2u}	210
211	F_{1u} – TO	$\longrightarrow$	E_u	164
126	F_{2u}	$\rightleftarrows$	A_{1u} E_u	148 132
542	R_1	$\longrightarrow$	A_{2g}	513
341	R_{10}	$\rightleftarrows$	A_{1u} E_u	327 330
445	R_3	$\longrightarrow$	E_g	412 (465)
188	R_4	$\rightleftarrows$	A_{2g} E_g	190 198 (260)
65*i*	R_5	$\rightleftarrows$	A_{1g} E_g	79 (180) 34

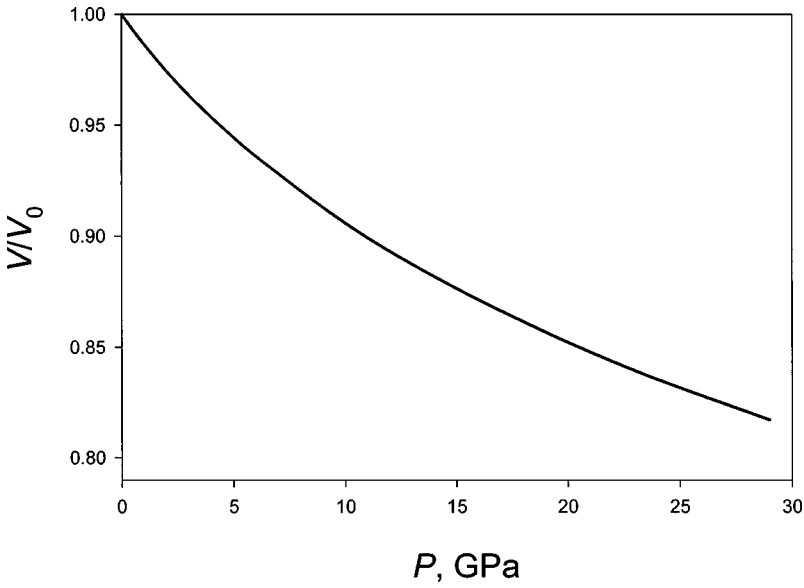

Figure 8. Calculated equation of state for ScF_3.

natural to attribute the first observed phase transition at $P \approx 0.7$ GPa to this mode condensation.

Figure 9 shows calculated dependence of squared frequency of this mode $\omega^2(R_5)$ on the unit cell volume. Under volume decrease (pressure growing) $\omega^2(R_5)$ goes down linearly and comes to zero at $P \approx 2.5$ GPa. Lower experimental value of transition pressure may be due to structural defects, that are known to destabilize MeF_3 cubic phase [7].

Eigenvector of this critical R_5 mode corresponds to ScF_6 octahedron rotation around body diagonal of the cubic cell [18]. This irreducible representation appears in the vibrational presentation only once; therefore it's possible to express $\omega^2(R_5)$ analytically using elements of dynamic matrix, and separate contributions of long-range Coulomb interactions of ions (ω_C^2) and of shorter range interactions (ω_S^2—these include dipole-dipole and higher multipoles interactions):

$$\omega^2(R_5) = \omega_C^2 + \omega_S^2, \tag{4}$$

These components may be further separated into:

$$\omega_C^2 = L_C - T_C; \quad \omega_S^2 = L_S - T_S, \tag{5}$$

$$L = D^{xx}_{F_1-F_1}\left(\mathbf{q} = \frac{\pi}{a}(1,1,1)\right), \tag{6}$$

$$T = D^{yz}_{F_1-F_2}\left(\mathbf{q} = \frac{\pi}{a}(1,1,1)\right), \tag{7}$$

where L corresponds to longitudinal, and T to transversal force constants of F–F interactions. Figure 9 demonstrates dependences of the values (5–7) on the cell volume. It's clearly seen that Coulomb and short-range components of $\omega^2(R_5)$ are of different signs and the long-range component prevails at ambient pressure, stabilizing the cubic phase structure. Both components increase under pressure, but the short-range one grows quicker and induces mode softening and lattice instability. Figure 9(b) demonstrates that this drastic growth of the short-range component is mainly connected with dipole-dipole interactions participating into $D^{xx}_{F_1-F_1}(\mathbf{q} = \frac{\pi}{a}(1,1,1))$ element of dynamic matrix.

Condensation of R_5 mode results in rhombohedric distortion of the crystal lattice that stabilizes new structure. Figure 10 shows crystal energy at $P = 6$ GPa as the function of fluorine displacements from their cubic

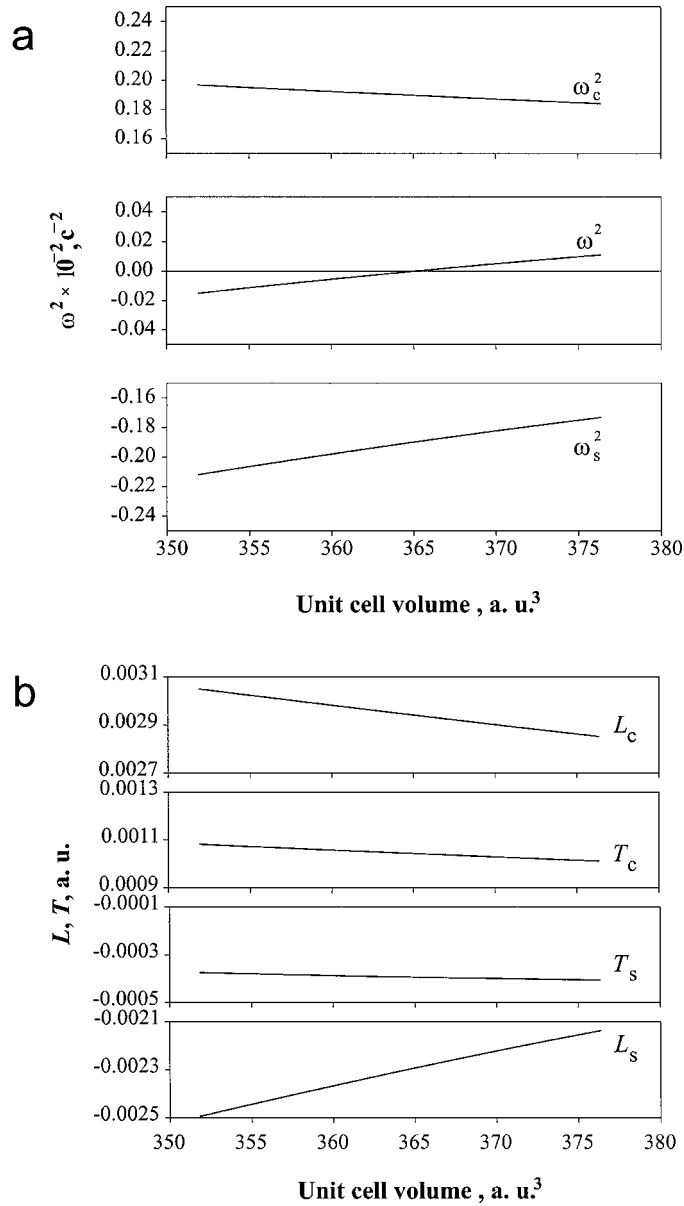

Figure 9. Calculated squared frequency of the soft mode R_5 (a) and corresponding elements of dynamic matrix (b) as a function of unit cell volume.

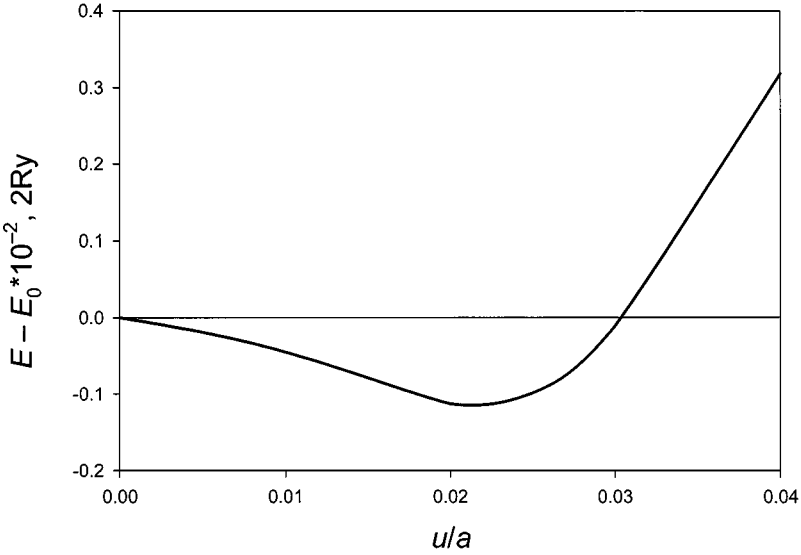

Figure 10. Energy of the crystal (per double cubic cell) as a function of fluorine atoms' displacement from their equilibrium positions in the cubic lattice. $E_0 = -2148.9854$, 2Ry is the energy of undistorted phase.

positions:

$$\tilde{u}^x_{\mathrm{F}_1} = -\tilde{u}^y_{\mathbf{F}_1} = \tilde{u}^y_{\mathbf{F}_2} = -\tilde{u}^z_{\mathbf{F}_2} = -\tilde{u}^x_{\mathbf{F}_3} = \tilde{u}^z_{\mathbf{F}_3} = u, \tag{8}$$

$$\tilde{u}^\alpha_{\mathbf{F}_1} = \frac{\tilde{u}^\alpha_{\mathbf{F}_1}}{2a} \exp(\mathrm{i}\mathbf{q}_\mathrm{R}\mathbf{r}), \tag{9}$$

here a is the cubic cell parameter; $\mathbf{r} = m_1\mathbf{a}_1 + m_2\mathbf{a}_2 + m_3\mathbf{a}_3$ the lattice translation vector, $\mathbf{q}_\mathrm{R} = \frac{\pi}{a}(1,1,1)$. Energy minimum corresponds to displacements $u \approx 0{,}025a$ (0.7 Å).

Table II shows calculated phonon frequencies for center of Brillouin zone of the rhombohedric phase; these optimal atomic positions (8) were taken for simulation. In the same table frequencies at $\Gamma(\mathbf{q} = (0,0,0))$ and $R(\mathbf{q} = \frac{\pi}{a}(1,1,1))$ points of the cubic phase are given.

Four Raman lines should activate above first transition point (see Eq. (2)); two of them ($A_{1\mathrm{g}}$ and E_g) correspond to restoring soft mode and split after the transition. Therefore they should be of lower frequencies and grow under further compressing. Three lines observed experimentally (their frequencies

are given in Table II in brackets) fit well to this description; the lowest of them shifts up considerably with pressure, while lower frequency wing appearing above transition may be attributed to the second restoring mode somewhere below 150 cm^{-1}. It should be pointed out as well, that the experimental frequencies correlate well with Raman scattering data for rhombohedric phases of other MeF_3 crystals [19]. So we can conclude that the first high pressure phase is rhombohedric, with $R\bar{3}c$, $Z = 2$ structure.

Second transition point, 3.8 GPa, as well as its essentially first order character with strong hysteresis, agree well with the value of rhombohedric to orthorhombic (*Pnma*, $Z = 4$) transition, observed earlier [7]. It is consistent with observed sharp appearance of a number of new Raman lines (3). Authors of [7] reported about strong diffuse X-ray scattering above this transition point, that slowly weakened under further compression; this correlates with appearance of complicated domain structure, observed under the microscope, and growing of these domains' size under compression.

CONCLUSION

So in this paper we've performed experimental investigations and numerical simulations of ScF_3 crystal under hydrostatic pressure.

Observed structural phase transition from cubic to rhombohedric phase at 0.7 GPa agrees with results of *ab initio* simulations that showed cubic lattice stability at ambient pressure with unusually low phonon branch between R and M points of Brillouin zone. Under lattice compression this branch progresses further down and induces lattice instability. Such frequency shift and lattice instability is driven by disbalance of Coulomb and short-range interactions within fluorine sublattice.

Calculated phonon spectrum of resulting rhombohedric phase agrees with the experimental one, where one soft mode restoration has been observed. The second restoring soft mode is supposed to be below 150 cm^{-1}, out of studied frequency range.

Transition pressure and character of the second transition point (strong hysteresis effects, complicated domain structure giving rise for strong X-ray and light scattering) to the orthorhombic phase agree well with the one observed in [7]; Raman spectra of this high pressure phase has been obtained for the first time. Symmetry of this phase corresponds to further condensation of the same soft branch but additional investigations are necessary to verify this possibility and are in progress now.

ACKNOWLEDGEMENTS

We'd like to thank Dr. A. P. Shebanin for his help during experimental measurements. This work has been supported by grants INTAS 97-10177 and the Russian Foundation for Basic Research 00-02-17792, 02-02-97707. One of us (SAG) wishes to thank financial support from CRDF (grant REC-008) and the Russian Foundation for Basic Research (grant 02-05-65313).

REFERENCES

[1] Ph. Daniel, A. Bulou, M. Rousseau, J. Nouet, J. L. Fourquet, M. Leblanc, and R. Burriel, *J. Phys. Condens. Matter* **2**, 5663 (1990).
[2] K. A. Aleksandrov, A. T. Anistratov, B. V. Beznosikov, and N. V. Fedoseeva, *Phase Transitions in ABX_3 Crystals* (Novosibirsk, Nauka Publishers, 1981) (in Russian).
[3] D. Babel and A. Tressaud, *Crystal Chemistry of Fluorides*. In *Inorganic Solid Fluorides* (London e. a., Academic Press, 1985), p. 77.
[4] Powder Diffraction Data, nos. 75-0877, 46-1243, 44-1096, 43-1145, 32-0989, 17-0836 (Int. Center Diffr. Data, USA, 1999).
[5] M. M. Aleksandrova, N. A. Bendeliany, V. D. Blank, and T. I. Dyuzheva, *Inorganic Materials* **26**, 1028 (1990) (in Russian).
[6] V. I. Zinenko and N. G. Zamkova, *Phys. Solid State* **42**, 1348 (2000).
[7] N. A. Bendeliany, E. Ya. Atabaeva, and V. M. Agotkov, *Inorganic Materials* **19**, 816 (1983) (in Russian).
[8] K. S. Aleksandrov, V. N. Voronov, A. Bulou, A. Robert, P. Daniel, and B. Hennion, *Abstracts of 6th Japan-CIS Symposium on Ferroelectricity* (Noda, Japan, 1998), p. 152.
[9] K. S. Aleksandrov, V. N. Voronov, A. N. Vtyurin, S. A. Goryainov, N. G. Zamkova, V. I. Zinenko, and A. S. Krylov, *J. Exper. Theor. Phys.* **94**, 977 (2002).
[10] B. M. Wanklyn, *J. Crystal Growth* **5**, 279 (1969).
[11] B. M. Wanklyn, *J. Mater. Sci.* **14**, 1447 (1979).
[12] V. A. Timofeeva, *Crystals Growth from Flux Melts* (Nauka Publishers, Moscow, 1978) (in Russian).
[13] Q. Wang, G. Ripault, and A. Bulou, *Phase Transitions* **53**, 1 (1995).
[14] S. V. Goryainov and I. A. Belitsky, *Phys. Chem. Minerals* **22**, 443 (1995).
[15] R. G. Munro, G. J. Piermarini, S. Block, and W. B. Holzapfel, *J. Appl. Phys.* **57**, 165 (1985).
[16] O. V. Ivanov and E. G. Maksimov, *J. Exper. Theor. Phys.* **108**, 1841 (1995).
[17] V. I. Zinenko, N. G. Zamkova, and S. N. Sofronova, *J. Exper. Theor. Phys.* **111**, 1742 (1998).
[18] R. Cowley, *Phys. Rev.* **134**, 981 (1964).
[19] P. Daniel, A. Bulou, M. Rossieau, J. Nouet, and M. Leblanc, *Phys. Rev.* **B** 42, 10545 (1990).